Check for updates

Novel synthetic approach to the preparation of single-phase $Bi_xLa_{1-x}MnO_{3+\delta}$ solid solutions

Dovydas Karoblis[1] · Kestutis Mazeika[2] · Dalis Baltrunas[2] · Anna Lukowiak[3] · Wieslaw Strek[3] · Aleksej Zarkov[1] · Aivaras Kareiva[1]

Abstract

In this study, the $Bi_xLa_{1-x}MnO_{3+\delta}$ solid solutions (x from 0 to 0.65) were synthesized using sol–gel combustion method with citric acid as a fuel and complexing agent. It was shown that changes in chemical composition of the materials lead to the evolution of crystal structure, morphology, and magnetic properties. The thermal behavior of precursor gel was investigated by thermogravimetric and differential scanning calorimetry (TG-DSC) measurements. X-ray diffraction (XRD) analysis demonstrated that all samples were monophasic. The Rietveld analysis showed that the structure can be indexed by trigonal or cubic unit cell depending on Bi^{3+} content. Scanning electron microscopy (SEM) was used to evaluate morphological features of the synthesized materials and revealed that Bi^{3+} ions significantly promote growth of the grains. The sol–gel-derived $Bi_xLa_{1-x}MnO_{3+\delta}$ specimens were also characterized by FT-IR spectroscopy and magnetization measurements, which showed a clear correlation between magnetic properties and crystal structure of the materials.

Graphical Abstract

Magnetization versus magnetic field curves for $Bi_xLa_{1-x}MnO_{3+\delta}$ solid solutions
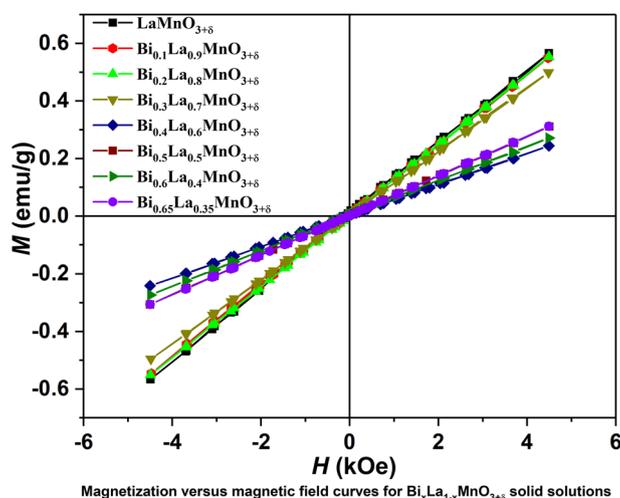
✉ Aleksej Zarkov
  aleksej.zarkov@chf.vu.lt

1   Institute of Chemistry, Vilnius University, Naugarduko 24, LT-03225 Vilnius, Lithuania

2   State Research Institute Center for Physical Sciences and Technology, LT-02300 Vilnius, Lithuania

3   Institute of Low Temperature and Structure Research, Polish Academy of Sciences, Okolna 2, PL-50422 Wroclaw, Poland

⁂ Springer

1 Introduction

Multiferroic materials that exhibit two or more "ferroic" (ferromagnetism, ferroelasticity, and ferroelectricity) properties at once recently were deeply investigated [1–4]. These materials offer new areas of applications, such as AC/DC magnetic field sensors, microwave resonators, and new data storage media [5, 6]. $LaMnO_3$ perovskite is a material, which exhibits interesting magnetic, ferromagnetic, magnetocaloric, and electrical properties [7–10]. By substituting La^{3+} with similar ionic radius and isovalent Bi^{3+}, the multiferroic $BiMnO_3$ perovskite was obtained showing the possibility of coexistence of both ferromagnetism and ferroelectricity [11, 12].

The crystal structure of stoichiometric $LaMnO_3$ at room temperature is orthorhombic. This material is antiferromagnetic insulator with good electrical conductivity and chemical stability at high temperatures [13, 14]. Depending on the synthesis temperature, duration of heating, and atmosphere, the oxygen content in the $LaMnO_3$ perovskite structure can differ [15–18]. The excess of oxygen is usually explained as cationic vacancies. The $LaMnO_{3+\delta}$ material has orthorhombic structure when $0 \leq \delta \leq 0.06$, and becomes rhombohedral when $0.10 \leq \delta \leq 0.18$. Between the 0.06 and 0.10 regions, the sample with $\delta = 0.07$ exhibits reflections of both phases in the X-ray diffraction (XRD) patterns [17]. The crystal structure of $BiMnO_3$ at room temperature is monoclinic [19, 20]. $BiMnO_3$ shows ferromagnetism below 100 K [21] and $LaMnO_3$ exhibits antiferromagnetism at 160 K [13]. The Mn–O plane in $BiMnO_3$ and $LaMnO_3$ demonstrates similar electron bonding state and spin arrangement. The different ferroelectric ordering is caused by different degree of electron localization on the La–O and Bi–O planes [22].

Despite $LaMnO_3$ could be easily synthesized using different synthetic approaches, the synthesis of monophasic $BiMnO_3$ at ambient conditions is very problematic. However, the substitution of Bi^{3+} by La^{3+} ions can lead to smaller distortions and lower synthesis temperatures during the preparation of Bi-rich $Bi_xLa_{1-x}MnO_3$ solid solutions [22]. Quite a few articles have been reported regarding the $Bi_xLa_{1-x}MnO_3$ system prepared by solid state reaction [23–27] or by pulsed laser deposition [28]. The maximum substitution level of 0.65 at ambient conditions was observed [25]. The higher amount of Bi^{3+} resulted in the formation of Bi_2O_3 impurity phase [27]. It is interesting to note, that the transition to ferromagnetic

insulating state was observed for the samples with $x = 0.2$ and 0.25 [27]. There is no clear correlation between amount of Bi^{3+} and changes in crystal structure. The transition from rhombohedral to pseudocubic cell was observed at $x = 0.5$ [27]. However, the transition from orthorhombic to cubic structure when $x = 0.3$ [23] or from rhombohedral to trigonal structure for $x = 0.4$ [25] were also reported. Besides, different magnetic and transport properties of $Bi_xLa_{1-x}MnO_3$ solid solutions with different amount of Bi^{3+} ions were determined as well [23–27].

Sol–gel combustion method is simple, time- and cost-effective synthetic approach providing high homogeneity and stoichiometry control of the products. Different fuels and fuel to oxidant ratios can be used in order to obtain nano-sized powders with controllable morphological features [29, 30]. Previously this method was successfully utilized for the synthesis of high-quality single [31, 32] and mixed-metal oxide materials [33–35] with magnetic and electrical properties. Different bi- and tri-metallic manganites with magnetic properties were also prepared by sol–gel combustion using glycine–nitrate method [36–38]. However, in all these reports starting materials were dissolved in a certain amount of solvent, which leads to more time-consuming synthetic procedure. The remarkable feature of our proposed synthesis method is that no external solvent was used. All precursor salts were dissolved in water released from starting crystal hydrates, which led to the synthesis in minimal volume and, consequently, reduced synthesis time.

In this study, the monophasic $Bi_xLa_{1-x}MnO_{3+\delta}$ compounds ($x = 0.0–0.65$) were prepared for the first time by simple environmentally friendly aqueous sol–gel combustion synthesis route using citric acid as complexing agent and fuel without addition of external solvent. The structural, magnetic, and morphological properties of $Bi_xLa_{1-x}MnO_{3+\delta}$ solid solutions depending on the substitutional level of Bi^{3+} are also discussed in this study.

2 Experimental

2.1 Synthesis

For the preparation of $Bi_xLa_{1-x}MnO_{3+\delta}$ samples by sol–gel combustion synthesis route lanthanum(III) nitrate hexahydrate

($La(NO_3)_3·6H_2O$, Alfa Aesar, 99.9%), manganese(II) nitrate tetrahydrate ($Mn(NO_3)_2·4H_2O$, Alfa Aesar, 99.9%), bismuth (III) nitrate pentahydrate ($Bi(NO_3)_3·5H_2O$, Roth, 98%), and citric acid monohydrate ($C_6H_8O_7·H_2O$, Chempur, 99.9%) were used as starting materials. Citric acid monohydrate was used as a complexing agent and fuel for the self-burning reaction. The appropriate amounts of metal nitrates and citric acid monohydrate (the ratio between metal nitrates and citric acid monohydrate was 1:0.83 [39]) were mixed in a beaker at 80 °C until crystalline water was released and clear solution was formed. The obtained mixture was stirred for 1 h, afterwards the sol was transformed into transparent gel by slow evaporation of water at 100 °C. In this stage of sol–gel processing, the temperature of the hot plate was increased to 250 °C and spontaneous ignition process took place. Finally, the ashes were collected and annealed in a furnace for 6 h at 1000 °C in air atmosphere with a heating rate of 5 °C/min.

2.2 Characterization

The thermal decomposition of precursor gel was investigated by thermogravimetric and differential scanning calorimetry (TG-DSC) analysis using PerkinElmer STA 6000 Simultaneous Thermal Analyzer. A total of 5–10 mg of dried sample was heated from 30 °C to 900 °C at 10 °C/min heating rate in a dry flowing air (20 mL/min). XRD analysis of obtained products were performed with Miniflex II diffractometer (Rigaku) using a primary beam Cu K_α radiation ($\lambda = 1.541838$ Å). The 2Θ angle of the diffractometer was set in the range from 10° to 80° in steps of 0.02°, with the measuring time of 0.4 s per step. The obtained diffraction data were refined by the Rietveld method using the Fullprof suite. PerkinElmer FT-IR spectrometer was used for FT-IR analysis of compounds. All spectra were recorded at ambient temperature in the range of 4000–400 cm^{-1}. The morphology of samples was examined using a scanning electron microscope (SEM) Hitachi SU-70. The vibrating sample magnetometer was applied for the magnetization measurements. The compounds were encapsulated into a plastic straw and placed into the magnetometer. The lock-in amplifier SR510 was used for measurement of the signal from the sense coils generated by vibrating sample. The gauss/teslameter FH-54 was used to measure the magnetic field strength between the poles of the laboratory magnet, which was supplied by the power source SM 330-AR-22.

3 Results and discussion

The $Bi_xLa_{1-x}MnO_{3+\delta}$ compounds ($x = 0.0$–0.65) were synthesized by heating the appropriate La–Bi–Mn–O precursor gel. The thermal decomposition behavior of Bi
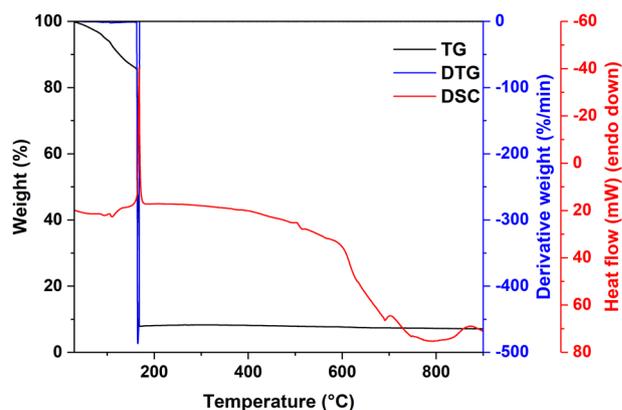

Fig. 1 TG-DSC curves of Bi(0.6)–La(0.4)–Mn–O dried gel

(0.6)–La(0.4)–Mn–O dried gel was investigated using TG-DSC measurements in order to determine the decomposition steps and possible final annealing temperature (Fig. 1). The first mass loss (about 15%) in the TG curve was observed in the temperature range of 30–160 °C and could be attributed to the removal of residual water. The small endotherm in the DSC curve peaked at about 110 °C also indicates this process. It can be seen that thermal decomposition of Bi (0.6)–La(0.4)–Mn-O gel occurs in one main step, which can be associated with combustion reaction. Sharp exothermic peak can be observed at 164 °C in the DSC curve confirming that combustion reaction occurs during thermal degradation of the gel. With further increasing of temperature the mass is nearly constant. After the reaction the total weight of the sample decreased at about 92%.

Figure 2 represents the XRD patterns of sol–gel-derived $Bi_xLa_{1-x}MnO_{3+\delta}$ compounds. It is evident that all synthesized compounds are monophasic and no even traces of impurity phases are present at higher Bi^{3+} concentrations, as was reported previously [23, 25, 27]. The Rietveld refinement of the XRD data confirmed the formation of trigonal perovskite structure with hexagonal setting $R\bar{3}c$, which was previously reported [9, 40]. The same space group and crystallographic structure were observed for the samples with $x = 0.1$–0.3. As the amount of Bi^{3+} increased, the shift of all diffraction peaks to lower 2θ values region was observed. Moreover, the intensity of less intense diffraction lines (204), (300), (217), (218), (321), and (330) monotonically decreases, until these peaks completely vanish at $x = 0.4$. From this point the perovskite structure can be indexed by cubic cell with $Pm\bar{3}m$ space group. The diffraction peaks (200), (201), and (301) start to split when Bi^{3+} concentration is reached 0.65. This should indicate another structural change, but the sample can still be fitted according to the cubic cell. Taking into account that $BiMnO_3$ is monoclinic, it is expected that symmetry should be further divergent from cubic with further increasing Bi^{3+} amount from 0.65 to 1.0.

All refined lattice parameters and Mn–O bond lengths for the synthesized samples are presented in Table 1. It is clearly seen that Mn–O bond length, cell parameters and cell volume are slightly different for the samples with different substitutional level of bismuth. These changes probably are caused by slightly different ionic radius of Bi^{3+} (1.17 Å) and La^{3+} (1.16 Å) in eightfold coordination [41]. The parameter a decreases as x increases until $x = 0.2$. The similar trend was also observed in ref. [23]. The value of parameter a abruptly increases when x reaches 0.3. The observed increase in p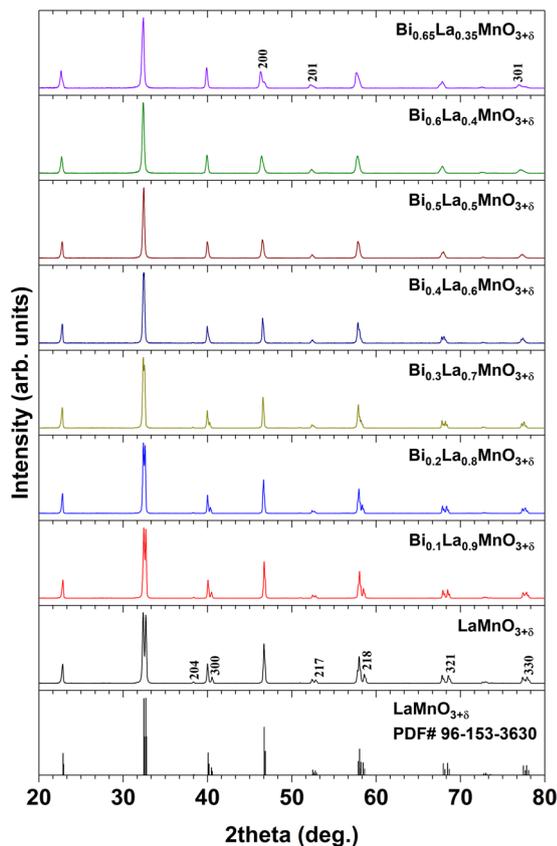arameter c in trigonal structure is nearly linear. In the cubic cell the increase of parameter a also can be seen. By comparing the determined cell volumes of cubic and trigonal cells we can conclude that volume in trigonal cell is about six times larger than in cubic cell. In addition, the cell volume increases almost linearly with increasing amount of Bi^{3+} in both types of cells.

Figure 3 represents FT-IR analysis data of fabricated $Bi_xLa_{1-x}MnO_{3+\delta}$ samples. In perovskite-like ABO_3 structure, cations La^{3+} and Bi^{3+} occupy A sites and Mn^{3+} ions B sites. Six oxygen O^{2-} anions and one manganese cation are forming MnO_6 octahedron. There are six possible vibration modes for this octahedron (three of them are stretching and three of them are vibrating modes) [42]. Only two modes (one bending and one stretching) are infrared active, with frequencies about 600 and 350 cm^{-1}, respectively [43]. The FT-IR spectra presented in Fig. 3 clearly show the absorption bands at 560–575 cm^{-1} attributable to the Mn–O stretching vibration in MnO_6. However, no correlation between the changes in Mn–O bond length and vibration frequencies in FT-IR spectra was observed.

The morphology of the synthesized $Bi_xLa_{1-x}MnO_{3+\delta}$ powders was examined using SEM. The SEM micrographs of the representative $Bi_xLa_{1-x}MnO_{3+\delta}$ samples with $x = 0$, 0.3, 0.6, and 0.65 are shown in Fig. 4. The $LaMnO_{3+\delta}$ solids are composed of the polyhedral particles varying in size in the range of ~100–200 nm (Fig. 4a). These particles form "dimers" or even "oligomers" showing negligible
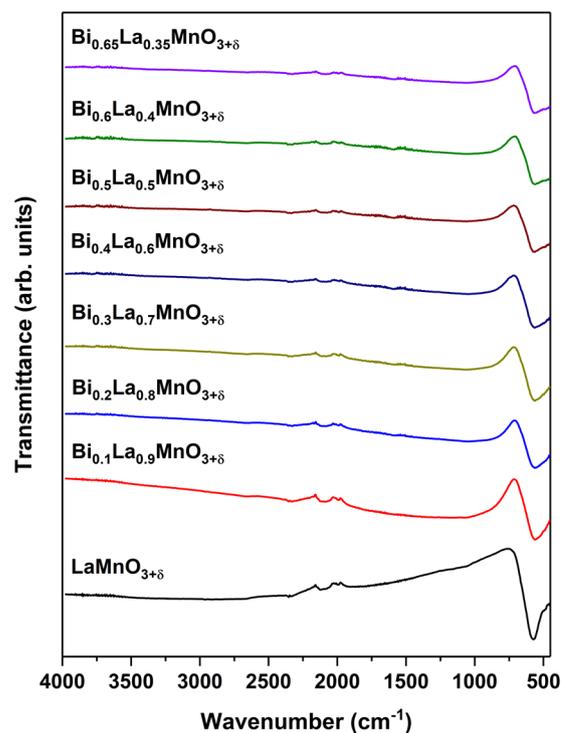
Fig. 2 XRD patterns of $Bi_xLa_{1-x}MnO_{3+\delta}$ powders obtained at 1000 °C

Fig. 3 FT-IR spectra of $Bi_xLa_{1-x}MnO_{3+\delta}$ samples

Table 1 Lattice parameters of $Bi_xLa_{1-x}MnO_{3+\delta}$ samples

x	a (Å)	b (Å)	c (Å)	V (Å³)	Mn–O (Å)
0	5.5158 (8)	5.5158 (8)	13.3234 (2)	351.05 (5)	1.9524
0.1	5.5124 (4)	5.5124 (4)	13.3584 (2)	351.53 (9)	1.9600
0.2	5.5120 (6)	5.5120 (6)	13.3760 (8)	351.95 (5)	1.9607
0.3	5.5164 (8)	5.5164 (8)	13.408 (8)	353.38 (3)	1.9566
0.4	3.8960 (9)	3.8960 (9)	3.8960 (9)	59.14 (1)	1.9480
0.5	3.8998 (6)	3.8998 (6)	3.8998 (6)	59.31 (2)	1.9499
0.6	3.9010 (7)	3.9010 (7)	3.9010 (7)	59.36 (8)	1.9505
0.65	3.9070 (8)	3.9070 (8)	3.9070 (8)	59.64 (3)	1.9535

Fig. 4 SEM micrographs of
LaMnO$_{3+\delta}$ (**a**), Bi$_{0.3}$La$_{0.7}$MnO$_{3+\delta}$
(**b**), Bi$_{0.6}$La$_{0.4}$MnO$_{3+\delta}$ (**c**), and
Bi$_{0.65}$La$_{0.35}$MnO$_{3+\delta}$ (**d**) samples
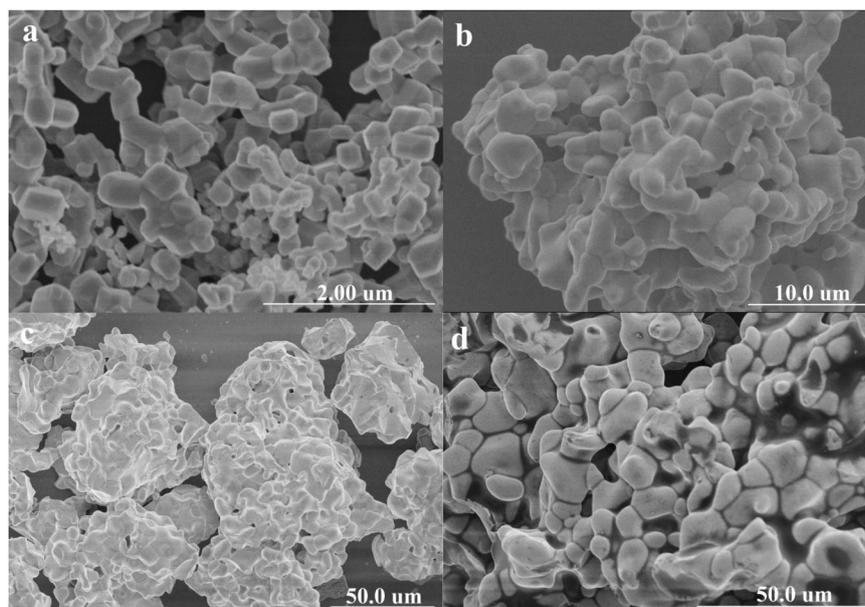
association and interaction between the grains. It is clearly
seen that partial substitution of lanthanum ions by bismuth
changes morphology of the powders. Two trends associated
with an introduction of bismuth into crystal lattice were
observed—first, increase in bismuth content promotes gra-
dual growth of the grains. The second trend is that the
particles in the bismuth containing compounds have lost the
strict shape and show high tendency for agglomeration. The
size of individual grains in Bi$_{0.65}$La$_{0.35}$MnO$_{3+\delta}$ increased up
to 5–10 μm (Fig. 4d).

The magnetization studies were also carried out for the
Bi$_x$La$_{1-x}$MnO$_{3+\delta}$ samples. The corresponding hysteresis
curves are represented in Fig. 5. For the LaMnO$_{3+\delta}$ sample
the Curie transition from ferromagnetic to paramagnetic
phase occurs at 140–180 K interval [9, 27, 44]. The M–H
loops for the sol–gel-derived Bi$_x$La$_{1-x}$MnO$_{3+\delta}$ samples
obtained at room temperature are linear, which correspond
with previous reported data and indicate the paramagnetic
state for all samples. Also, no saturation of magnetization
was observed at applied magnetic field. From Fig. 5, we can
clearly see that magnetization for trigonal structure is about
2–3 times higher than magnetization in cubic structure. It
seems that structural transition causes the change in mag-
netic properties of Bi$_x$La$_{1-x}$MnO$_{3+\delta}$ as well. The magneti-
zation is clearly different determined for the Bi$_{0.3}$La$_{0.7}$MnO$_{3+\delta}$
and Bi$_{0.4}$La$_{0.6}$MnO$_{3+\delta}$ samples. For trigonal cell magnetiza-
tion decreases with increasing amount of Bi^{3+} negligibly,
with only exception for $x = 0.1$, which is a little higher than
for observed for the sample with $x = 0.2$ sample. There is no
clear dependence between magnetization and bismuth content
in highly doped Bi$_x$La$_{1-x}$MnO$_{3+\delta}$ samples (x from 0.4 to
0.65) with cubic crystal structure as well. The magnetization
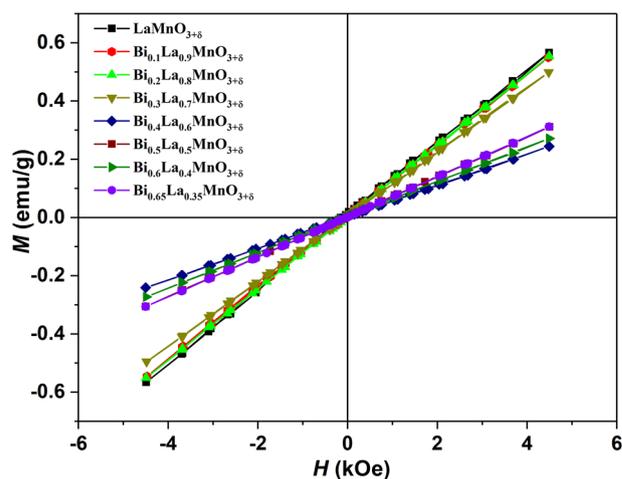
Fig. 5 Magnetization versus magnetic field curves for Bi$_x$La$_{1-x}$MnO$_{3+\delta}$
samples

values vary insignificantly. Different amount of bismuth in
the crystal lattice, grain size or morphology of the powders do
not show any obvious trends.

4 Conclusions

The formation of monophasic solid solutions of
Bi$_x$La$_{1-x}$MnO$_{3+\delta}$ in the range of $x = 0.0$–0.65 has been
demonstrated. These single-phase compounds were pre-
pared for the first time by simple, rapid, and environmen-
tally friendly sol–gel combustion method which does not
require an addition of external solvent. The TG-DSC mea-
surements of the Bi-La-Mn-O precursor gels showed that

combustion reaction occurred during thermal degradation of the gels. The results of XRD analysis showed that synthesized $Bi_xLa_{1x}MnO_{3+\delta}$ powders with $x = 0.0$–0.3 showed trigonal crystal structure with space group $R\overline{3}c$. With increasing amount of bismuth, the transformation of crystal cell to cubic $Pm\overline{3}m$ space group took place. The SEM micrographs of sol–gel-derived $Bi_xLa_{1x}MnO_{3+\delta}$ samples showed that microstructure of the materials also depends on chemical composition. The samples with higher Bi^{3+} content had obviously larger grains. The magnetization measurements demonstrated that all samples were paramagnetic and no saturation of magnetization at applied magnetic fields was observed. The structural changes from trigonal to cubic cell resulted in decrease of magnetization.

Compliance with ethical standards

Conflict of interest The authors declare that they have no conflict of interest.

Publisher's note: Springer Nature remains neutral with regard to jurisdictional claims in published maps and institutional affiliations.

References

1. Dong S, Liu JM, Cheong SW, Ren ZF (2015) Multiferroic materials and magnetoelectric physics: symmetry, entanglement, excitation, and topology. Adv Phys 64(5–6):519–626. https://doi.org/10.1080/00018732.2015.1114338

2. Fiebig M, Lottermoser T, Meier D, Trassin M (2016) The evolution of multiferroics. Nat Rev Mater 1(8):14. https://doi.org/10.1038/natrevmats.2016.46

3. Lakshmi SD, Banu IBS (2019) Multiferroism and magnetoelectric coupling in single-phase Yb and X (X = Nb, Mn, Mo) co-doped $BiFeO_3$ ceramics. J Sol-Gel Sci Technol 89(3):713–721. https://doi.org/10.1007/s10971-018-4901-x

4. Song Gl SuJ, Yang H, Zhang N, Chang F (2018) Modified crystal structure, dielectric properties, and magnetic phase transition temperature of Ca doped $BiFeO_3$ ceramic. J Sol-Gel Sci Technol 85(2):421–430. https://doi.org/10.1007/s10971-017-4541-6

5. Vopson MM (2015) Fundamentals of multiferroic materials and their possible applications. Crit Rev Solid State Mat Sci 40(4):223–250. https://doi.org/10.1080/10408436.2014.992584

6. Wang T, Song S-H, Wang X-L, Chen J-J, Tan M-L (2018) Chemical substitution-induced structure transition and enhanced magnetic and optical properties of sol–gel synthesized multiferroic $BiFeO_3$ nanoparticles. J Sol-Gel Sci Technol 85(2):356–368. https://doi.org/10.1007/s10971-017-4552-3

7. Liu YK, Wong HF, Lam KK, Mak CL, Leung CW (2019) Tuning ferromagnetic properties of $LaMnO_3$ films by oxygen vacancies and strain. J Magn Magn Mater 481:85–92. https://doi.org/10.1016/j.jmmm.2019.03.001

8. Das R, Midya A, Kumari M, Chaudhuri A, Yu XJ, Rusydi A, Mahendiran R (2019) Enhanced magnetocaloric effect driven by hydrostatic pressure in Na-doped $LaMnO_3$. J Phys Chem C 123(6):3750–3757. https://doi.org/10.1021/acs.jpcc.8b09964

9. Iqbal M, Khan MN, Khan AA (2018) Structural, magnetic, magnetocaloric and critical behavior studies in the vicinity of the paramagnetic to ferromagnetic phase transition temperature in $LaMnO_{3+delta}$ compound. J Magn Magn Mater 465:670–677. https://doi.org/10.1016/j.jmmm.2018.06.026

10. Chiabrera F, Garbayo I, Pla D, Burriel M, Wilhelm F, Rogalev A, Nunez M, Morata A, Tarancon A (2019) Unraveling bulk and grain boundary electrical properties in $La_{0.8}Sr_{0.2}Mn_{1-yO3 +/-delta}$ thin films. APL Mater 7(1):8. https://doi.org/10.1063/1.5054576

11. Chou CC, Huang CL, Mukherjee S, Chen QY, Sakurai H, Belik AA, Takayama-Muromachi E, Yang HD (2009) Multiple magnetic transitions in multiferroic $BiMnO_3$. Phys Rev B 80(18):6. https://doi.org/10.1103/PhysRevB.80.184426

12. Lee BW, Yoo PS, Nam VB, Toreh KRN, Jung CU (2015) Magnetic and electric properties of stoichiometric $BiMnO_3$ thin films. Nanoscale Res Lett 10:5. https://doi.org/10.1186/s11671-015-0759-9

13. Iliev MN, Litvinchuk AP, Abrashev MV, Ivanov VG, Lee HG, McCarroll WH, Greenblatt M, Meng RL, Chu CW (2000) Raman monitoring of the dynamical Jahn-Teller distortions in rhombohedral antiferromagnetic $LaMnO_3$ and ferromagnetic magnetoresistive $La_{0.98}Mn_{0.96}O_3$. Physics C 341:2257–2258. https://doi.org/10.1016/s0921-4534(00)01103-5

14. Hosseini SA, Mehri B, Niaei A, Izadkhah B, Alvarez-Galvan C, Fierro JGL (2018) Selective catalytic reduction of NO_x by CO over $LaMnO_3$ nano perovskites prepared by microwave and ultrasound assisted sol–gel method. J Sol-Gel Sci Technol 85(3):647–656. https://doi.org/10.1007/s10971-017-4568-8

15. Alonso JA, MartinezLope MJ, Casais MT, MacManusDriscoll JL, deSilva P, Cohen LF, FernandezDiaz MT (1997) Non-stoichiometry, structural defects and properties of $LaMnO_{3+\delta}$ with high δ values ($0.1<=\delta<=0.29$). J Mater Chem 7(10):2139–2144. https://doi.org/10.1039/a704088a

16. Kamata K, Nakajima T, Hayashi T, Nakamura T (1978) Non-stoichiometric behavior and phase stability of rare earth manganites at 1200 °C: (1). LaMnO3 Mater Res Bull 13(1):49–54. https://doi.org/10.1016/0025-5408(78)90026-0

17. Topfer J, Goodenough JB (1997) $LaMnO_{3+\delta}$ revisited. J Solid State Chem 130(1):117–128. https://doi.org/10.1006/jssc.1997.7287

18. Tola PS, Kim HS, Kim DH, Phan TL, Rhyee JS, Shon WH, Yang DS, Manh DH, Lee BW (2017) Tunable magnetic properties and magnetocaloric effect of off-stoichiometric $LaMnO_3$ nanoparticles. J Phys Chem Solids 111:219–228. https://doi.org/10.1016/j.jpcs.2017.07.022

19. Belik AA, Iikubo S, Yokosawa T, Kodama K, Igawa N, Shamoto S, Azuma M, Takano M, Kimoto K, Matsui Y, Takayama-Muromachi E (2007) Origin of the monoclinic-to-monoclinic phase transition and evidence for the centrosymmetric crystal structure of $BiMnO_3$. J Am Chem Soc 129(4):971–977. https://doi.org/10.1021/ja0664032

20. Acharya SA, Gaikwad VM, Kulkarni SK, Despande UP (2017) Low pressure synthesis of $BiMnO_3$ nanoparticles: anomalous structural and magnetic features. J Mater Sci 52(1):458–466. https://doi.org/10.1007/s10853-016-0345-2

21. Sugawara F, Iiida S, Syono Y, Akimoto S-i (1968) Magnetic properties and crystal distortions of $BiMnO_3$ and $BiCrO_3$. J Phys Soc Jpn 25(6):1553–1558. https://doi.org/10.1143/JPSJ.25.1553

22. Multiferroic Materials (2017). CRC Press, Boca Raton. https://doi.org/10.1201/9781315372532

23. Joseph DP, Lin JW, Kumar NP, Chen WC, Lin JG (2016) Isovalent Bi3+ substitution induced structural and magnetic transitions in LaMnO3 J Magn Magn Mater 418:68–75. https://doi.org/10.1016/j.jmmm.2016.02.003

24. Lin YQ, Wu YJ, Gu SP, Chen XM (2009) Contribution of electron hopping on colossal dielectric response of Bi-substituted LaMnO$_3$ ceramics. Ferroelectrics 388:133–139. https://doi.org/10.1080/00150190902966800

25. Troyanchuk IO, Mantytskaja OS, Szymczak H, Shvedun MY (2002) Magnetic phase transitions in the system La$_{1-x}$Bi$_x$MnO$_{3+\lambda}$. Low Temp Phys 28(7):569–573. https://doi.org/10.1063/1.1496669

26. Zhang HG, Li YT, Dong XG, Hou QT, Huang YC, Liu H, Li Q (2013) X-ray absorption spectroscopy and photoemission study of Bi-doped LaMnO$_3$. J Phys Conf Ser 430. https://doi.org/10.1088/1742-6596/430/1/012072

27. Zhao YD, Park J, Jung RJ, Noh HJ, Oh SJ (2004) Structure, magnetic and transport properties of La$_{1-x}$Bi$_x$MnO$_3$. J Magn Magn Mater 280(2–3):404–411. https://doi.org/10.1016/j.jmmm.2004.06.024

28. Gajek M, Bibes M, Wyczisk F, Varela M, Fontcuberta J, Barthelemy A (2007) Growth and magnetic properties of multiferroic La$_x$Bi$_{1-x}$MnO$_3$ thin films. Phys Rev B 75(17):7. https://doi.org/10.1103/PhysRevB.75.174417

29. Zarkov A, Stanulis A, Salkus T, Kezionis A, Jasulaitiene V, Ramanauskas R, Tautkus S, Kareiva A (2016) Synthesis of nanocrystalline gadolinium doped ceria via sol–gel combustion and sol–gel synthesis routes. Ceram Int 42(3):3972–3988. https://doi.org/10.1016/j.ceramint.2015.11.066

30. Nikolić D, Panjan M, Blake GR, Tadić M (2015) Annealing-dependent structural and magnetic properties of nickel oxide (NiO) nanoparticles in a silica matrix. J Eur Ceram Soc 35(14):3843–3852. https://doi.org/10.1016/j.jeurceramsoc.2015.06.024

31. Kopanja L, Milosevic I, Panjan M, Damnjanovic V, Tadic M (2016) Sol–gel combustion synthesis, particle shape analysis and magnetic properties of hematite (α-Fe2O3) nanoparticles embedded in an amorphous silica matrix. Appl Surf Sci 362:380–386. https://doi.org/10.1016/j.apsusc.2015.11.238

32. Tadic M, Nikolic D, Panjan M, Blake GR (2015) Magnetic properties of NiO (nickel oxide) nanoparticles: blocking temperature and Neel temperature. J Alloy Compd 647:1061–1068. https://doi.org/10.1016/j.jallcom.2015.06.027

33. Tadic M, Savic SM, Jaglicic Z, Vojisavljevic K, Radojkovic A, Prsic S, Nikolic D (2014) Magnetic properties of NiMn$_2$O$_{4-\delta}$ (nickel manganite): multiple magnetic phase transitions and exchange bias effect. J Alloy Compd 588:465–469. https://doi.org/10.1016/j.jallcom.2013.11.025

34. Zarkov A, Mikoliunaite L, Katelnikovas A, Tautkus S, Kareiva A (2018) Preparation by different methods and analytical characterization of gadolinium-doped ceria. Chem Pap 72(1):129–138. https://doi.org/10.1007/s11696-017-0264-y

35. Zarkov A, Stanulis A, Sakaliuniene J, Butkute S, Abakeviciene B, Salkus T, Tautkus S, Orliukas AF, Tamulevicius S, Kareiva A (2015) On the synthesis of yttria-stabilized zirconia: a comparative study. J Sol-Gel Sci Technol 76(2):309–319. https://doi.org/10.1007/s10971-015-3778-1

36. Markovic D, Kusigerski V, Tadic M, Blanusa J, Antisari MV, Spasojevic V (2008) Magnetic properties of nanoparticle La0.7Ca0.3MnO3 prepared by glycine–nitrate method without additional heat treatment. Scr Mater 59(1):35–38. https://doi.org/10.1016/j.scriptamat.2008.02.020

37. Markovic D, Kusigerski V, Tadic M, Blanusa J, Jaglicic Z, Cvjeticanin N, Spasojevic V (2010) The influence of the heat treatment on the structural and magnetic properties of nanoparticle La0.7Ca0.3MnO3 prepared by glycine–nitrate method. J Alloy Compd 494(1):52–57. https://doi.org/10.1016/j.jallcom.2010.01.062

38. Tadić M, Marković D, Panjan M, Spasojević V (2016) Solution combustion synthesis method and magnetic properties of synthesized polycrystalline calcium manganite CaMnO3−δ powder. Ceram Int 42(16):19365–19371. https://doi.org/10.1016/j.ceramint.2016.09.109

39. Jain SR, Adiga KC, Verneker VRP (1981) A new approach to thermochemical calculations of condensed fuel-oxidizer mixtures. Combust Flame 40(1):71–79. https://doi.org/10.1016/0010-2180(81)90111-5

40. Barnabe A, Gaudon M, Bernard C, Laberty C, Durand B (2004) Low temperature synthesis and structural characterization of over-stoichiometric LaMnO$_{3+delta}$ perovskites. Mater Res Bull 39(4–5):725–735. https://doi.org/10.1016/j.materresbull.2003.10.008

41. Shannon RD (1976) Revised effective ionic radii and systematic studies of interatomic distances in halides and chalcogenides. Acta Crystallogr Sect A 32(SEP1):751–767. https://doi.org/10.1107/s0567739476001551

42. Nakamoto K (2001) Infrared and raman spectra of inorganic and coordination compounds. Handbook of vibrational spectroscopy. https://doi.org/10.1002/0470027320.s4104

43. Kebin L, Xijun L, Kaigui Z, Jingsheng Z, Yuheng Z (1997) Infrared absorption spectra of manganese oxides La$_{1-x-y}$R$_y$-Ca$_x$MnO$_{3-\delta}$. J Appl Phys 81(10):6943–6947. https://doi.org/10.1063/1.365234

44. Atsarkin VA, Demidov VV, Balbashov AM (2004) Anomalous slowing down of the longitudinal spin relaxation near the antiferromagnetic phase transition in LaMnO$_3$ manganite. JETP Lett 80(9):593–596. https://doi.org/10.1134/1.1851641